Stars and their variability observed from space
C. Neiner, W. W. Weiss, D. Baade, R. E. Griffin, C. C. Lovekin, A. F. J. Moffat (eds)

NEW FULLY EVOLUTIONARY MODELS FOR ASTEROSEISMOLOGY OF ULTRA-MASSIVE WHITE-DWARF STARS

A. H. Córsico[1,2], F. C. De Gerónimo[1,2], M. E. Camisassa[1,2] and L. G. Althaus[1,2]

Abstract. Ultra-massive hydrogen-rich white dwarf (WD) stars of spectral type DA ($M_\star > 1M_\odot$) coming from single-star evolution are expected to harbour cores made of ^{16}O and ^{20}Ne, resulting from semi-degenerate carbon burning when the progenitor star evolved through the super-asymptotic giant branch phase. These stars are expected to be crystallized by the time they reach the ZZ Ceti instability strip ($T_{\rm eff} \sim 12\,500$ K). Theoretical models predict that crystallization leads to a separation of ^{16}O and ^{20}Ne in the core of ultra-massive WDs, which has an impact on their pulsational properties. That property offers a unique opportunity to study the processes of crystallization. This paper presented the first results of a detailed asteroseismic analysis of the best-studied ultra-massive ZZ Ceti star, BPM 37093. As a second step, we plan to repeat the analysis using ultra-massive DA WD models with C/O cores in order to study the possibility of elucidating the core chemical composition of BPM 37093 and shed some light on its evolutionary origin. We also plan to extend this kind of analysis to other stars observed from the ground and with space instruments like *Kepler* and *TESS*.

Keywords: tars: pulsations, interiors, white dwarfs

1 Input physics, evolution/pulsation codes, and stellar models

In this project, evolutionary models were generated by Camisassa et al. (2019) employing the `LPCODE` evolutionary code. They are shown in Fig. 1. The input physics of `LPCODE` is described by Camisassa et al. (2019), where details can be found. Of particular importance in this work is the treatment of crystallization. Cool WD stars are believed to crystallize through the strong Coulomb interactions in their very dense interiors (van Horn 1968). In our models, crystallization set in when the energy of the Coulomb interaction between neighbouring ions was much higher than their thermal energy. The release of latent heat, and the release of gravitational energy associated with changes in the chemical composition profile induced by crystallization, were taken into account consistently. The chemical redistribution due to phase separation and the associated release of energy were considered following Althaus et al. (2010), appropriately modified by (van Horn 1968) for ONe plasmas. To assess the enhancement of ^{20}Ne in the crystallized core, we used the azeotropic-type phase diagram of Medin & Cumming (2010). The pulsation code used to compute nonradial g(gravity)-mode pulsations was the adiabatic version of the `LP-PUL` pulsation code described by Córsico & Althaus (2006). To account for the effects of crystallization on the pulsation spectrum of g modes, we adopted the "hard sphere" boundary conditions (see Montgomery & Winget 1999). Our ultra-massive WD models have stellar masses $M_\star = 1.10, 1.16, 1.22$, and $1.29M_\odot$. They result from the complete evolution of the progenitor stars through the super-asymptotic giant branch phase. The core and inter-shell chemical profiles of our models at the start of the WD cooling phase were obtained from Siess (2010).

2 Chemical profiles and the Brunt-Väisälä frequency

The cores of our models are composed mostly of ^{16}O and ^{20}Ne, plus and smaller amounts of ^{12}C, ^{23}Na, and ^{24}Mg. Since element diffusion and gravitational settling operate throughout the WD evolution, our models develop pure H envelopes. The He content of our WD sequences is given by the evolutionary history of progenitor star, but instead, the H content of our canonical envelopes [$\log(M_{\rm H}/M_\star) = -6$] has been set by imposing that the further evolution does not lead to H thermonuclear flashes on the WD cooling track. We have expanded our grid

[1] Facultad de Ciencias Astronómicas y Geofísicas, Universidad Nacional de La Plata, Paseo delBosque s/n, (1900), La Plata, Argentina
[2] Instituto de Astrofísica de La Plata, IALP, CONICET-UNLP, La Plata, Argentina

© Stars from Space

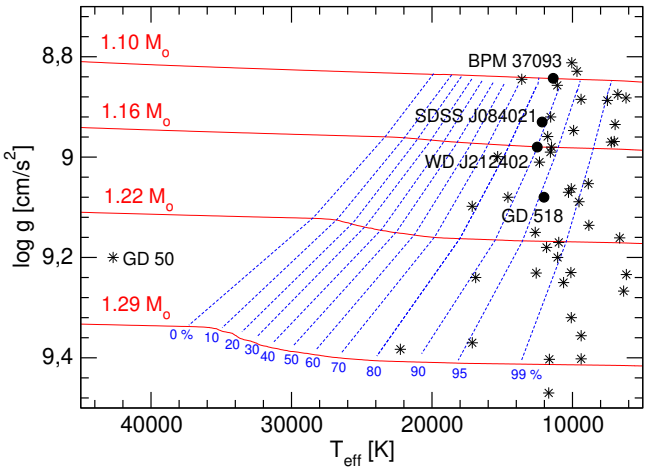

Fig. 1. Evolutionary tracks (red solid lines) of the ultra-massive DA WD models computed by Camisassa et al. (2019) in the $T_{\rm eff}$ – – $\log g$ plane. Blue dashed lines indicate 0, 10, 20, 30, 40, 50, 60, 70, 80, 90, 95 and 99% of crystallized mass. The location of ultra-massive DA WD stars are indicated by black star symbols, and the ultra-massive ZZ Ceti stars are shown as black dots.

of models by generating new sequences artificially with thinner H envelopes [$\log(M_{\rm H}/M_\star) = -7, -8, -9, -10$], for each value of stellar mass. This procedure was done at high-luminosity stages of the WD evolution. The temporal changes of the chemical abundances due to element diffusion were assessed by using a new fully-implicit treatment for time-dependent element diffusion (Althaus et al. 2019, submitted).

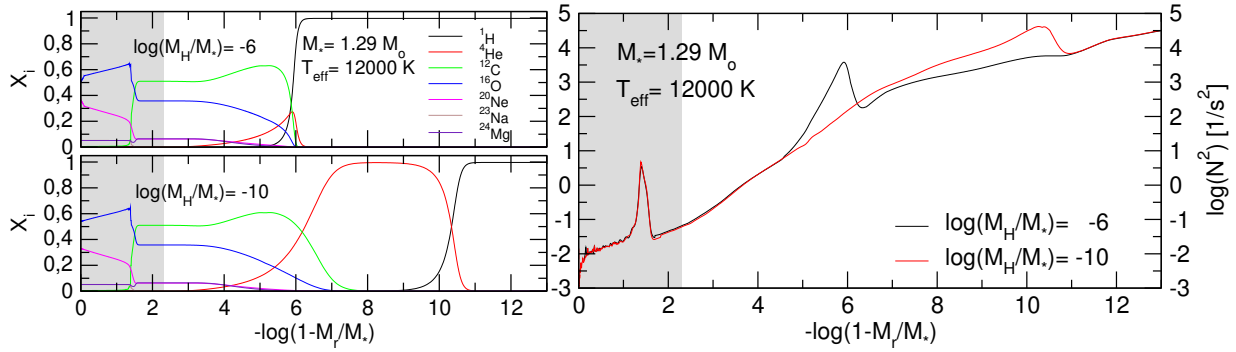

Fig. 2. Left: Abundances of the different chemical species by mass, as a function of the fractional mass, corresponding to ONe-core WD models with $M_\star = 1.29 M_\odot$, $T_{\rm eff} \sim 12\,000$ K and two different H-envelope thicknesses, as indicated. The percentage of crystallized mass fraction of the models is 99.5% (grey region). **Right:** Logarithm of the squared Brunt-Väisälä frequency, corresponding to the same ONe-core WD models with $M_\star = 1.29 M_\odot$, $T_{\rm eff} \sim 12\,000$ K and $\log(M_{\rm H}/M_\star) = -6$, and -10 that are shown in the left panel.

The chemical profiles in terms of the fractional mass for $1.29 M_\star$ ONe-core WD models at $T_{\rm eff} \sim 12\,000$ K and H envelope thicknesses $\log(M_{\rm H}/M_\star) = -6$ and -10 are shown in the left panel of Fig. 2. A pure He buffer develops as we consider thinner H envelopes. At this effective temperature, the chemical rehomogenization due to crystallization has already finished, giving rise to a core where the abundance of ^{16}O (^{20}Ne) increases (decreases) outwards. The right panel of Fig. 2 shows the logarithm of the squared Brunt-Väisälä frequency corresponding to the same models shown in the left panel. The peak at $-\log(1 - M_r/M_\star) \sim 1.4$, which is due to the abrupt step at the triple chemical transition between ^{12}C, ^{16}O and ^{20}Ne, is within the solid part of the core, so it has no relevance for the mode-trapping properties of the models. This is because, according to the hard-sphere boundary conditions adopted for the pulsations, the eigenfunctions of g modes do not penetrate the crystallized region. In this way, the mode-trapping properties are entirely determined by the presence of the He/H transition, which is located in more external regions for thinner H envelopes. The pulsation properties of these models have been explored by De Gerónimo et al. (2019) and Córsico et al. (2019, submitted).

Table 1. Frequencies and periods of BPM 37093 (Metcalfe et al. 2004), together with the theoretical periods, harmonic degrees, radial orders and period differences of our best-fitting model.

$\Pi^{\rm O}$ [sec]	ν [μHz]	$\Pi^{\rm T}$ [sec]	ℓ	k	δ_i [sec]
511.7	1954.1	512.4	2	29	−0.7
531.1	1882.9	531.9	1	17	−0.8
548.4	1823.5	548.1	2	31	0.3
564.1	1772.7	565.3	2	32	−1.2
582.0	1718.2	583.0	2	33	−1.0
600.7	1664.9	599.9	2	34	0.8
613.5	1629.9	613.8	1	20	−0.3
635.1	1574.6	632.2	2	36	2.9

Table 2. The main characteristics of BPM 37093

Quantity	Spectroscopy	Asteroseismology
$T_{\rm eff}$ [K]	$11\,370 \pm 500$	$11\,650 \pm 40$
$M_\star/M_\odot$	1.098 ± 0.1	1.16 ± 0.014
$\log g$ [cm/s^2]	8.843 ± 0.05	8.970 ± 0.025
$\log(L_\star/L_\odot)$	—	-3.25 ± 0.01
$\log(R_\star/R_\odot)$	—	-2.234 ± 0.006
$\log(M_{\rm H}/M_\star)$	—	-6 ± 0.26
$\log(M_{\rm He}/M_\star)$	—	-3.8
$M_{\rm cr}/M_\star$	0.935	0.923
$X_{^{16}{\rm O}}$ cent.	—	0.52
$X_{^{20}{\rm Ne}}$ cent.	—	0.34
Quantity	Measured	Asteroseismology
$\overline{\Delta\Pi}_{\ell=1}$ [s]	—	29.70
$\overline{\Delta\Pi}_{\ell=2}$ [s]	17.3 ± 0.9	17.63
Quantity	Astrometry (*Gaia*)	Asteroseismology
d [pc]	14.81	11.32
π [mas]	67.5	88.3

3 Application: asteroseismological analysis of the ultra-massive ZZ'Ceti star BPM 37093

BPM 37093 is the first ultra-massive ZZ Ceti star discovered by Kanaan et al. (1992). It is characterized by $T_{\rm eff} = 11\,370$ K and $\log g = 8.843$ (Nitta et al. 2016). We searched for a pulsation model that matches the individual pulsation periods of BPM 37093 best. The goodness of the match between the theoretical pulsation periods ($\Pi_k^{\rm T}$) and the observed periods ($\Pi_i^{\rm O}$) is measured by means of a merit function defined as $\chi^2(M_\star, M_{\rm H}, T_{\rm eff}) = \frac{1}{N}\sum_{i=1}^{N} \min[(\Pi_i^{\rm O} - \Pi_k^{\rm T})^2]$, where N is the number of observed periods. The WD model that shows the lowest value of χ^2, if it exists, is adopted as the "best-fitting model". We assumed two possibilities for the mode identification: (i) that all of the observed periods correspond to g modes with $\ell = 1$, and (ii) that the observed periods correspond to a mix of g modes with $\ell = 1$ and $\ell = 2$. We considered the eight periods employed by Metcalfe et al. (2004) (see Table 1). Case (i) did not show clear solutions compatible with BPM 37093 in relation to its spectroscopically-derived effective temperature. Rather, case (ii) resulted in a clear seismological solution for a WD model with $M_\star = 1.16 M_\odot$, $T_{\rm eff} = 11\,650$ K and $\log(M_{\rm H}/M_\star) = -6$. Table 1 shows the periods of the best-fitting model along with the harmonic degree, radial order, and the period differences (theoretical minus observed). Most of the periods of BPM 37093 were identified as $\ell = 2$ modes. That was not expected, owing to geometric cancellation effects (that is, $\ell = 1$ modes should be more easily detectable than $\ell = 2$ modes). Table 2 lists the main characteristics of the best-fitting model for BPM 37093. Its parameters are in agreement with the spectroscopically-derived ones. The asteroseismological distance is also in line with the astrometric distance obtained from *Gaia*.

A.H.C. warmly thanks the Local Organising Committee, in particular Prof. Werner W. Weiss, for support that allowed him to attend this conference.

References

Althaus, L. G., García-Berro, E., Renedo, I., et al. 2010, ApJ, 719, 612
Camisassa, M. E., Althaus, L. G., Córsico, A. H., et al. 2019, A&A, 625, A87
Córsico, A. H. & Althaus, L. G. 2006, A&A, 454, 863
De Gerónimo, F. C., Córsico, A. H., Althaus, L. G., Wachlin, F. C., & Camisassa, M. E. 2019, A&A, 621, A100
Kanaan, A., Kepler, S. O., Giovannini, O., & Diaz, M. 1992, ApJ, 390, L89
Medin, Z. & Cumming, A. 2010, Phys. Rev. E, 81, 036107
Metcalfe, T. S., Montgomery, M. H., & Kanaan, A. 2004, ApJ, 605, L133
Montgomery, M. H. & Winget, D. E. 1999, ApJ, 526, 976
Nitta, A., Kepler, S. O., Chené, A.-N., et al. 2016, IAU Focus Meeting, 29B, 493
Siess, L. 2010, A&A, 512, A10
van Horn, H. M. 1968, ApJ, 151, 227